J. Fluid Mech. (2007), *vol.* 586, *pp.* 371–396. © 2007 Cambridge University Press
doi:10.1017/S002211200700688X Printed in the United Kingdom

Growth and breakdown of low-speed streaks leading to wall turbulence

MASAHITO ASAI[1], YASUFUMI KONISHI[2], YUKI OIZUMI[2] AND MICHIO NISHIOKA[3]

[1]Department of Aerospace Engineering, Tokyo Metropolitan University, Asahigaoka 6-6, Hino, Tokyo 191-0065, Japan

[2]Department of Aerospace Engineering, Tokyo Metropolitan Institute of Technology, Asahigaoka 6-6, Hino, Tokyo 191-0065, Japan

[3]Graduate School of Engineering, Kyoto University, Yoshida-Honmachi, Sakyo-ku, Kyoto 606-8501, Japan

(Received 15 September 2005 and in revised form 26 April 2007)

Two-dimensional local wall suction is applied to a fully developed turbulent boundary layer such that near-wall turbulence structures are completely sucked out, but most of the turbulent vortices in the original outer layer can survive the suction and cause the resulting laminar flow to undergo re-transition. This enables us to observe and clarify the whole process by which the suction-surviving strong vortical motions give rise to near-wall low-speed streaks and eventually generate wall turbulence. Hot-wire and particle image velocimetry (PIV) measurements show that low-frequency velocity fluctuations, which are markedly suppressed near the wall by the local wall suction, soon start to grow downstream of the suction. The growth of low-frequency fluctuations is algebraic. This characterizes the streak growth caused by the suction-surviving turbulent vortices. The low-speed streaks obtain almost the same spanwise spacing as that of the original turbulent boundary layer without the suction even in the initial stage of the streak development. This indicates that the suction-surviving turbulent vortices are efficient in exciting the necessary ingredients for the wall turbulence, namely, low-speed streaks of the correct scale. After attaining near-saturation, the low-speed streaks soon undergo sinuous instability to lead to re-transition. Flow visualization shows that the streak instability and its subsequent breakdown occur at random in space and time in spite of the spanwise arrangement of streaks being almost periodic. Even under the high-intensity turbulence conditions, the sinuous instability amplifies disturbances of almost the same wavelength as predicted from the linear stability theory, though the actual growth is in the form of a wave packet with not more than two waves. It should be emphasized that the mean velocity develops the log-law profile as the streak breakdown proceeds. The transient growth and eventual breakdown of low-speed streaks are also discussed in connection with the critical condition for the wall-turbulence generation.

1. Introduction

With the idea that turbulence is caused and then sustained by a sequence of flow instabilities, we have been working on the transition to wall turbulence. For the case of wall-bounded flows, the instability events depend greatly on the disturbance environments, and various paths can lead to transition, even for the same flow

geometry. In any path to transition, however, the prerequisite for wall-turbulence generation is the occurrence and growth of near-wall low-speed streaks. Under very low free-stream turbulence, the boundary-layer transition is initially governed by the amplification of linear instability waves known as Tollmien–Schlichting waves and the low-speed streaks appear at the late stage of the secondary high-frequency instability. On increasing the intensity of background turbulence, the transition may skip the growth stage of Tollmien–Schlichting (T-S) waves. Such bypass transition is characterized by low-speed streaks, which can grow from the initial stage and eventually undergo lateral oscillations, often leading to the formation of turbulent spots. In the present study, our interest is focused on such near-wall phenomena to clarify the bypass transition and the wall turbulence mechanism.

As for the bypass transition caused by background turbulence, it has long been inferred that the streamwise streaks evolve from algebraic growth of non-modal disturbances known as transient growth (Landahl 1980; Hultgren & Gustavsson 1981). According to the related optimal disturbance analyses by Andersson, Berggren & Henningson (1999), Luchini (2000) and Tumin & Reshotko (2001), low-frequency or stationary streamwise streaks with a preferable spanwise wavelength about eight times the displacement thickness of the laminar boundary layer undergo the maximum spatial transient growth. Bypass transition experiments on a flat-plate boundary layer by Matsubara & Alfredsson (2001) showed that the disturbance growth, was not inconsistent with the transient growth, theory, though a notable difference was found in the spanwise scale of the low-speed streaks. By using roughness elements, White (2002) and Fransson *et al.* (2004) examined the transient growth for stationary disturbances and also found some deviation from the optimal theory in the disturbance profile and the streamwise development.

Asai & Nishioka (1995) investigated bypass transition in the response of a flat-plate boundary layer to energetic hairpin vortices excited periodically at the leading edge. The leading-edge-generated hairpin vortices decayed downstream. While rapidly decaying downstream, however, the hairpin vortices excited streamwise streaks as clearly visualized by smoke wire. Correspondingly, hot-wire measurements demonstrated the associated algebraic growth of u-fluctuations. The mean streak spacing was found to be about four times the displacement thickness, half that of the optimal disturbances.

When the near-wall low-speed streaks are intensified, they often undergo breakdown through lateral oscillations of a secondary instability nature. For the case of plane Poiseuille flow, on the basis of the linear stability analysis, Reddy *et al.* (1998) examined the threshold energy of disturbances for the streak breakdown leading to the transition at subcritical Reynolds numbers. A related experiment by Elofsson, Kawakami & Alfredsson (1999) showed that the occurrence of the secondary instability of streamwise streaks required a rather large amplitude of velocity variation across the low-speed streaks, for example, about 70 % of the centreplane velocity at a subcritical Reynolds number of 2000. Andersson *et al.* (2001) and Brandt *et al.* (2003) studied the instability of the optimal streaks numerically and analytically, respectively. Brandt & Henningson (2002) followed numerically the transition process caused by the streak instability up to the turbulent stage in a flat-plate boundary layer. Asai, Minagawa & Nishioka (2000, 2002) examined experimentally the instability of a single low-speed streak which was generated artificially by a small piece of wire-gauze screen set within a Blasius boundary layer to find that the varicose and sinuous modes can lead to the development of hairpin vortices with a pair of near-wall counter-rotating streamwise vortices and zigzag structure of quasi-streamwise vortices like those deduced by

Schoppa & Hussain (1997) in the DNS of the near-wall turbulence. Using the same apparatus, Konishi & Asai (2004) studied the stability of spanwise-periodic streaks by exciting subharmonic sinuous and varicose modes (with the periodicity of twice the streak spacing) as well as fundamental sinuous and varicose modes. Brandt (2007) reproduced the development of both the varicose and sinuous modes in a single streak numerically.

As for the transition initially controlled by the growth of T-S waves, on the other hand, a series of ribbon-induced transition experiments in plane channel flow by Nishioka, Asai & Iida (1981) and Nishioka & Asai (1984) demonstrated that immediately behind the hairpin vortices resulting from the secondary high-frequency instability, a single near-wall low-speed streak developed in between the neighbouring high-speed regions to undergo breakdown. They followed the flow development up to the beginning of the streak breakdown though they could not thoroughly clarify the whole instability process of the near-wall streak.

From DNS results for the so-called minimal flow unit for the wall turbulence, Jiménez & Moin (1991) demonstrated that the near-wall flow is dominated by mutually dependent low-speed streaks and streamwise vortices (inclined in the spanwise and normal-to-wall directions). Jeong *et al.* (1997) analysed DNS data by using a vortex identification technique (Jeong & Hussain 1995) to find a train of such dominant streamwise vortices. Through DNS of a minimal plane Couette flow at the lowest critical Reynolds number for sustaining wall turbulence, Hamilton, Kim & Waleffe (1995) clarified the regeneration cycle of low-speed streaks and streamwise vortices. The cycle is governed by the streak instability capable of generating zigzag structure of streamwise vortices of alternating sign. The streamwise vortices in turn accumulate low-speed fluids to form near-wall low-speed streaks, which soon undergo meandering wavy motions (namely, the streak instability), thus closing the regeneration cycle. If any of these events is interrupted, the flow is laminarized as shown by Jiménez & Pinelli (1999) through DNS of the developed channel flow turbulence. Kawahara & Kida (2001) identified the regeneration cycle in a turbulent Couette flow by finding time-periodic motions through a dynamical system approach. A similar travelling-wave solution corresponding to the nonlinear saturation stage of the streak instability was also found for a minimal channel flow by Itano & Toh (2001). Schoppa & Hussain (2002) emphasized that under high-intensity background turbulence such as in wall turbulence, a transient growth was more important for the breakdown of low-speed streaks than the normal-mode streak instability.

In the present transition study, we aim to obtain a better understanding of the self-sustaining mechanism of wall turbulence and the critical flow condition for its appearance. It is thus important to observe the development and the subsequent breakdown of low-speed streaks under well-controlled flow conditions. For this purpose, we apply two-dimensional local wall suction to a turbulent boundary layer. With the local suction, turbulent fluctuations near the wall can be significantly reduced or completely suppressed (see Antonia & Zhu 1995). However, most of turbulent vortices in the original outer layer can survive the suction and disturb the resulting laminar flow (without any streaks) to undergo re-transition in the same sense as in Narasimha & Sreenivasan (1973). We may expect that the surviving turbulent vortices might be the most efficient for exciting a sequence of instability events constituting the wall turbulence mechanism and enable us to clarify the whole process by which strong vortical motions excite near-wall low-speed streaks and eventually generate the wall turbulence. In addition, by changing the suction rate, we can examine the critical condition for the appearance of the wall turbulence mechanism. This is why

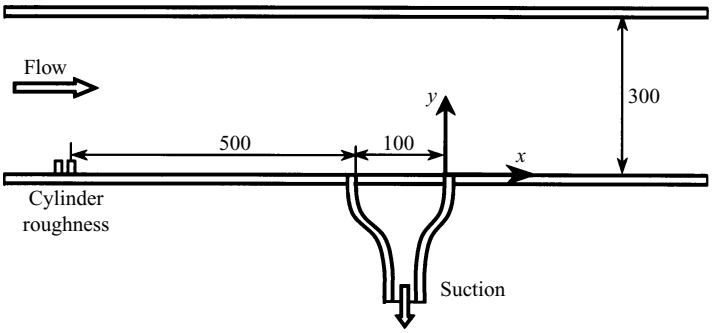

FIGURE 1. Schematic of the test section (dimensions in mm).

we observe the re-transition downstream of the wall suction. Our experiment is thus designed to observe various stages from the streak development to the eventual breakdown by adjusting the suction rate. With this experimental design, we expect that the regeneration process of near-wall low-speed streaks can be identified. The present study thus focuses attention on the key events governing the wall turbulence and the bypass transition.

2. Experimental set-up and procedure

The whole experiment is conducted in a wind tunnel with a rectangular test section of $300 \times 200\,\mathrm{mm}^2$ in cross-section. The wind tunnel has five 40-mesh damping screens and a honeycomb in the settling chamber of $750 \times 600\,\mathrm{mm}^2$. The contraction from settling chamber to test section is 7.5 in the area ratio. A schematic of the test section is given in figure 1. We focus on a boundary layer developing along the lower wall of the test section of 1100 mm in length. The free-stream velocity U_∞ is fixed at $4\,\mathrm{m\,s}^{-1}$ throughout the present experiment. The turbulence in the free stream, measured at the upstream end of the test section, is less than 0.15 % of U_∞. For the sake of low turbulence, the boundary layer remains laminar in the test section at $4\,\mathrm{m\,s}^{-1}$. To obtain a fully developed turbulent boundary-layer, circular cylinders are placed on the lower wall at the upstream end of the test section as an effective boundary-layer trip. The cylinder diameter and height are 3 mm and 4 mm respectively. They are glued to the wall in a two-row configuration. In each spanwise row, the cylinder spacing is 10 mm, and the two rows are separated by 10 mm in the streamwise direction and staggered by 5 mm in the spanwise direction.

The suction strip made of aluminium plate of 1.5 mm in thickness and $120 \times 180\,\mathrm{mm}^2$ in area is mounted flush with the wall surface. Over the suction area of $100 \times 160\,\mathrm{mm}^2$, 0.3 mm-diameter holes are drilled at an interval of 1 mm in the streamwise and spanwise directions in a staggered configuration. The porosity of the suction strip (the ratio of open to total areas) is 0.14. The leading edge of the suction area is located 500 mm downstream of the boundary-layer trip of cylinders in row. The suction strip is connected to a pump (a vacuum cleaner) through a smooth contraction, a pipe and a flow meter. The suction velocity can be controlled continuously up to a maximum speed of $2\,\mathrm{m\,s}^{-1}$ by means of two valves installed in the pipe system. Here, the suction velocity V_s is defined as $V_s = Q/A_s$ where Q and A_s denote the volumetric flow rate and the suction area ($100 \times 160\,\mathrm{mm}^2$), respectively. To check the uniformity of the suction, the z-distributions of time-mean streamwise velocity U are measured and we find it uniform over 70 % of the total

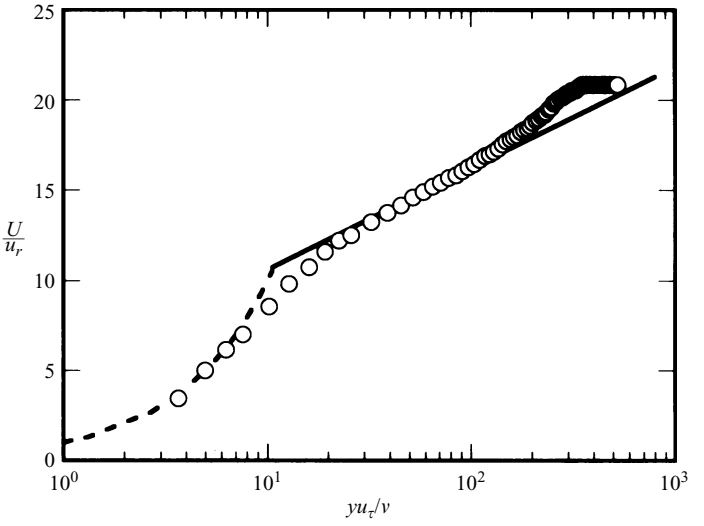

FIGURE 2. y-distributions of time-mean velocity U at $x = 50$ mm in the absence of suction. Solid line, $U/u_\tau = 5.62\log(yu_\tau/\nu) + 5.0$; broken line, $U/u_\tau = yu_\tau/\nu$.

suction area. When the boundary-layer suction is applied, the free-stream velocity outside the boundary layer is slightly decreased behind the suction area. For the case of $V_s/U_\infty = 10\,\%$, for instance, the free-stream velocity is decreased by 2.5 % at the x-stations downstream of the suction strip. For all the experiments with the boundary-layer suction, the free-stream velocity far upstream of the suction strip is set at $4\,\mathrm{m\,s^{-1}}$ as noted earlier. Our coordinate system is such that x is the streamwise distance, measured from the trailing edge of the suction strip (i.e. 500 mm downstream from the cylinder trip), y the normal-to-wall distance and z the spanwise distance.

The streamwise velocity, whose time-mean and fluctuation components are denoted by U and u, respectively, is measured with a constant-temperature hot-wire anemometer. The hot-wire sensor is 5 μm in diameter and 1 mm in length. The hot-wire probe is traversed in the x-, y- and z-directions. The y-distributions of U and u' (the root mean square (r.m.s.) value of u) are recorded on an XY plotter. The hot-wire signal is also stored in a personal computer. A particle image velocimetry (PIV) system (Dantec) which consists of a double-pulsed Nd:Yag laser and a CCD camera (HiSense) of 1280×1024 pixels is also used to obtain instantaneous velocity fields in the (x, z)-plane near the wall, with the seeding at the wind tunnel inlet. In addition, smoke-wire visualization is used to examine the development of near-wall low-speed streaks and their eventual breakdown. A smoke wire, stretched in the spanwise (z) direction, can be traversed in the x- and y-directions. Time sequences of top view and cross-sectional view pictures are taken by a high-speed digital video camera (Photron) with 1024×1024 pixels at a frame rate of 2000 frames $\mathrm{s^{-1}}$.

3. Flow fields with and without suction

In the absence of suction, the turbulent boundary layer caused by the cylinder trip is fully developed in the observation region, $x \geqq 0$. Figure 2 shows the y-distribution of time-mean velocity U measured at $x = 50$ mm, i.e. 650 mm downstream from the cylinder trip. The momentum thickness Reynolds number of the boundary layer R_θ is about 750 at $x = 50$ mm, and increases up to about 1000 at the most downstream

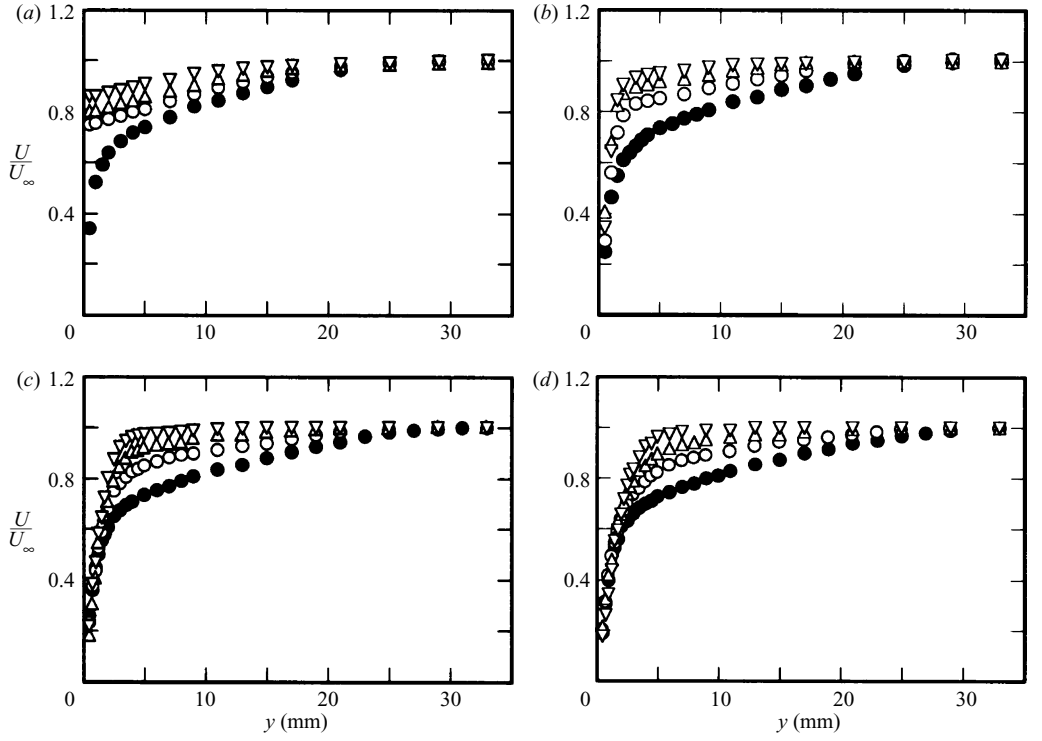

FIGURE 3. y-distributions of U for $V_s/U_\infty = 0\,\%$ (●), 5 % (○), 10 % (△) and 15 % (▽). (*a*) $x = -20$ mm; (*b*) $x = 50$ mm; (*c*) $x = 150$ mm; (*d*) $x = 250$ mm.

location of the observation region, $x = 400$ mm. The time-mean velocity exhibits the log-law profile. At $x = 50$ mm, the outer edge of the turbulent boundary layer is of about 300 in wall units defined by the friction velocity u_τ and the kinematic viscosity ν.

The boundary-layer suction is applied to the turbulent boundary layer over the streamwise region $-100\,\text{mm} \leqq x \leqq 0$. Figures 3 and 4, respectively, show the y-distributions of U and r.m.s. value of u-fluctuations u' at $x = -20$ mm, 50 mm, 150 mm and 250 mm for three cases of different suction velocities, $V_s/U_\infty = 5\,\%$, 10 % and 15 % by comparing them with the corresponding distributions without suction. Figures 3(*a*) and 4(*a*) indicate that the wall layer is completely sucked out even for the case of $V_s/U_\infty = 5\,\%$. The velocity fluctuation u' near the wall decreases to 6.5 % of U_∞ for the lowest suction velocity $V_s/U_\infty = 5\,\%$ (figure 4*a*). This value of u' is half the maximum value in the y-distribution of u', denoted by u'_m, without suction. For the highest suction velocity $V_s/U_\infty = 15\,\%$, the u'_m/U_∞ decreases to about 5.5 % at $x = -20$ mm, near the trailing edge of the suction strip. The effect of the wall suction on the mean velocity U is almost uniform over 70 % of the full span. The near-wall velocity fluctuations once suppressed by suction start to grow immediately downstream of the suction area (figures 4*b–d*). For $V_s/U_\infty = 5\,\%$ and 10 %, the magnitude of u'_m has already attained the value of the developed wall turbulence at $x = 150$ mm. For the case of $V_s/U_\infty = 15\,\%$, however, u'_m does not recover even at $x = 250$ mm and the re-transition to wall turbulence never occurs within the test section. Figure 5 shows the disturbance growth more clearly for $V_s/U_\infty = 5\,\%$, 10 % and 15 % by comparing the streamwise development of u'_m over $x = 20$–400 mm. For $V_s/U_\infty = 5\,\%$ and 10 %, we

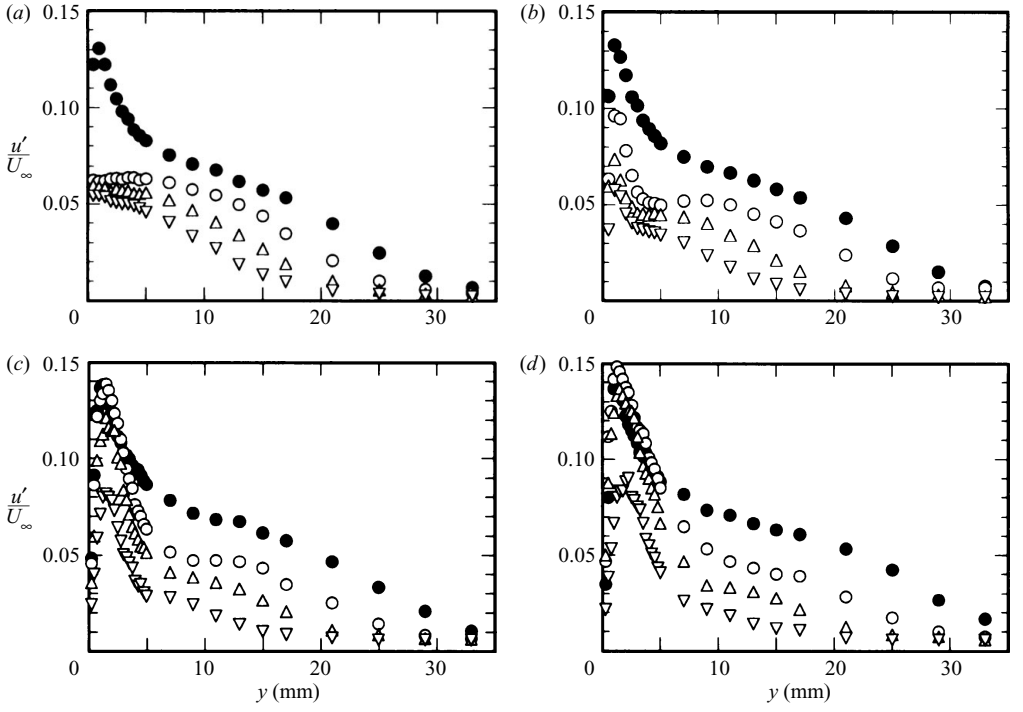

FIGURE 4. y-distributions of u' for $V_s/U_\infty = 0\,\%$ (●), $5\,\%$ (○), $10\,\%$ (△) and $15\,\%$ (▽). (*a*) $x = -20\,\text{mm}$; (*b*) $x = 50\,\text{mm}$; (*c*) $x = 150\,\text{mm}$; (*d*) $x = 250\,\text{mm}$.

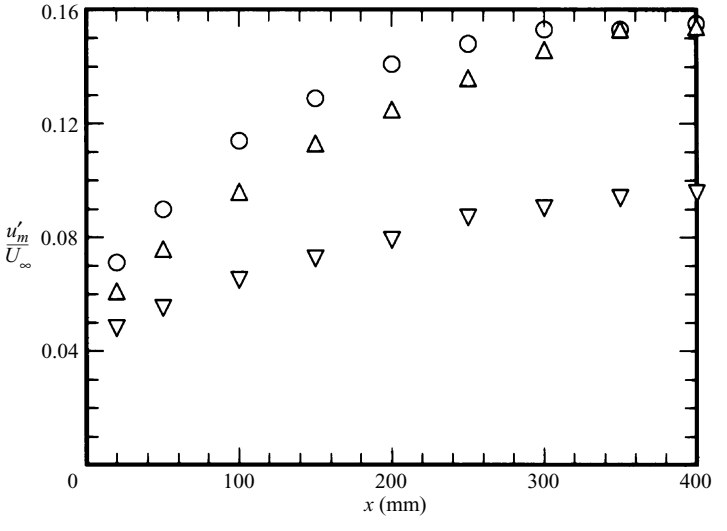

FIGURE 5. u'_m versus x for $V_s/U_\infty = 5\,\%$ (○), $10\,\%$ (△) and $15\,\%$ (▽).

see continuous growth of u-fluctuations up to $u'_m/U_\infty = 15\,\%$ within the test section. This growth leads to the recovery of the near-wall peak in the y-distributions of u' in figure 4. For $V_s/U_\infty = 15\,\%$, on the other hand, u'_m does not exceed $10\,\%$ of U_∞ even at the most downstream station $x = 400\,\text{mm}$.

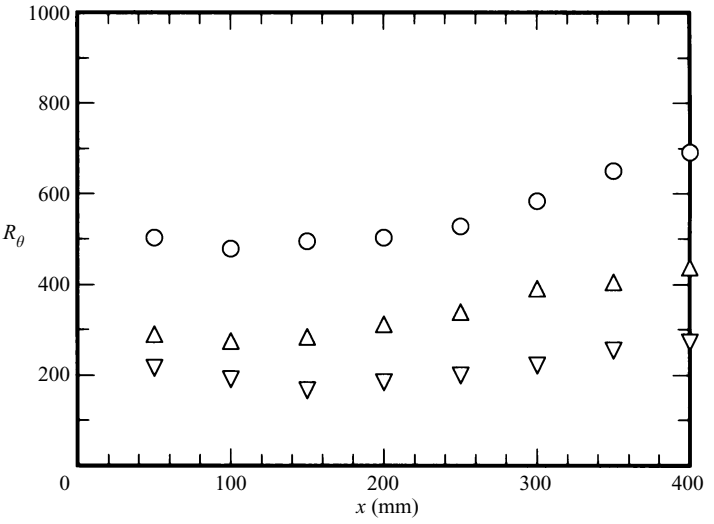

FIGURE 6. Reynolds number R_θ versus x for $V_s/U_\infty = 5\,\%$ (○), 10 % (△) and 15 % (▽).

Let us consider the cause for the different disturbance behaviours shown in figures 4 and 5. We know that the boundary-layer instability depends on the disturbance and the Reynolds number. As can be seen from figures 4(*a*) and 5, the type and magnitude of the initial disturbance are not much different for $V_s/U_\infty = 5\,\%$, 10 % and 15 %. This means that the Reynolds-number effect is the most important. The momentum thickness θ or the Reynolds number (based on θ) R_θ depends on the suction rate as shown in figure 6, which plots R_θ against x in the re-transition region. For $V_s/U_\infty = 15\,\%$, R_θ decreases to about 220 at $x = 50$ mm, immediately downstream of the suction. R_θ further decreases downstream, reaching a minimum of about 170 at $x = 150$ mm (about five times the boundary-layer thickness behind the suction) and remaining below 200 for $x = 100$–250 mm. Here, the decrease in R_θ observed downstream of the suction strip is caused by the suction-induced transfer of momentum towards the wall going on beyond the suction strip, just as observed by Antonia & Zhu (1995). By measuring the v-velocity field by PIV, we confirm the appearance of downward flow (negative v) downstream of the suction.

In connection with the Reynolds-number effect, the critical condition for the subcritical boundary-layer transition studied by Asai & Nishioka (1995, 1997) should be mentioned. In their experiment, the boundary-layer transition was triggered by high-intensity hairpin vortices excited near the leading edge. The critical R_θ for the occurrence of boundary-layer transition was found to be about 130, and the intensity of disturbances triggering the transition was only slightly less than that of the developed wall turbulence, i.e. about 10 % in terms of the maximum r.m.s. value u'_m/U_∞. In the present case, the turbulence level u'_m is about half that for the subcritical transition mentioned. Therefore, for the case of $V_s/U_\infty = 15\,\%$, it is understood that the triggering turbulence level is too low for the disturbance growth to lead to the re-transition. On the other hand, figure 6 shows that R_θ is above 490 and 270 for $V_s/U_\infty = 5\,\%$ and 10 %, respectively. For these cases, compared with the cited critical value 130, the Reynolds numbers are sufficiently high, and the triggering turbulence level for the occurrence of transition can be much lower than the threshold for the subcritical transition mentioned.

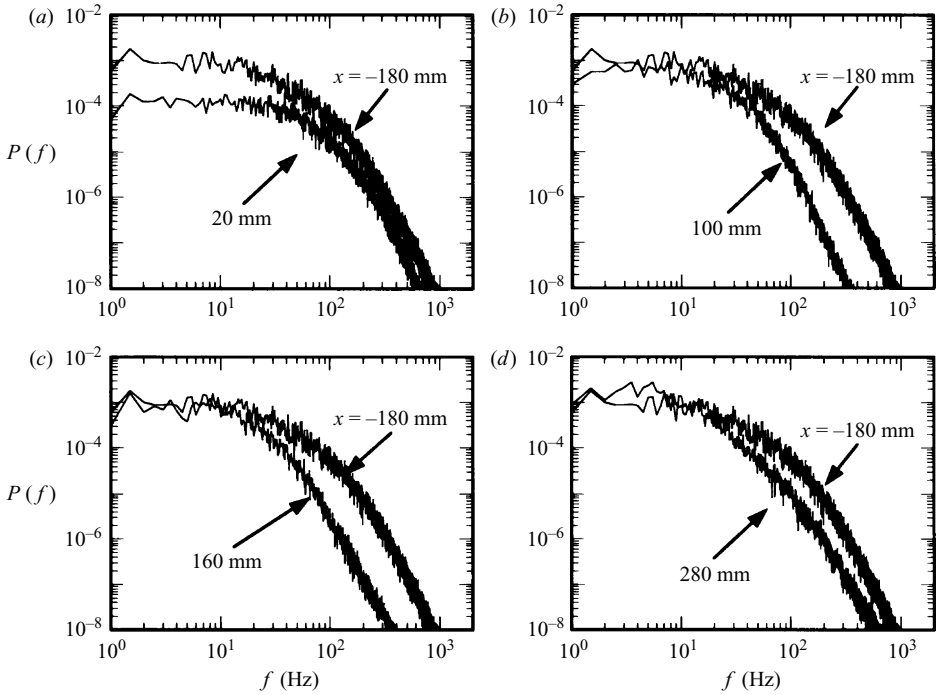

FIGURE 7. Power spectra of u-fluctuations measured at $y = 1$ mm for $V_s/U_\infty = 10\,\%$. (a) $x = 20$ mm; (b) $x = 100$ mm; (c) $x = 160$ mm; (d) $x = 280$ mm.

Figure 7 shows the power spectra of u-fluctuation $P(f)$ measured at $y = 1$ mm for the case of $V_s/U_\infty = 10\,\%$. The frequency resolution is 0.5Hz. The suction-induced re-laminarization is characterized by the fact that low-frequency fluctuations are markedly suppressed near the wall (see figure 7a). Downstream of the suction, the near-wall low-frequency fluctuations soon start to grow to attain the original level of the developed turbulence (see figure 7b–d). On the other hand, it is after passing through the suction area that the high-frequency fluctuations above 200 Hz start to decay appreciably. Importantly, even after the low-frequency components start to grow, the high-frequency components still keep decaying: compare figures 7(a) to 7(c). In order to see such different behaviour of the low- and high-frequency fluctuations more quantitatively, each frequency component is singled out from the power spectra $P(f)$ and its r.m.s. value is obtained. For instance, the r.m.s. value of the low-frequency component less than 25 Hz (and greater than 0.5 Hz), denoted by u'_{0-25}, is given as,

$$u'_{0-25} = \left(\int_{0.5}^{25} P(f)\,\mathrm{d}f \right)^{1/2}. \tag{3.1}$$

The r.m.s. values of frequency components, u'_{25-50}, u'_{50-75}, etc. are defined in the same manner. We obtain their x- and y-distributions for $V_s/U_\infty = 5\,\%$, $10\,\%$ and $15\,\%$. Figure 8(a) shows the streamwise development of u'_{0-25}, u'_{25-50}, u'_{50-75}, u'_{75-100} and $u'_{200-300}$ at $y = 1$ mm for the case of $V_s/U_\infty = 10\,\%$. The lowest-frequency component u'_{0-25} is suppressed down to about 3 % of U_∞ by suction, but immediately downstream of the suction it rapidly increases to approach the value of the developed turbulent boundary layer (without suction), $u'_{0-25}/U_\infty = 10\,\%$. On the other hand, the frequency components higher than 50 Hz keep decaying up to $x = 200$ mm. They start to grow

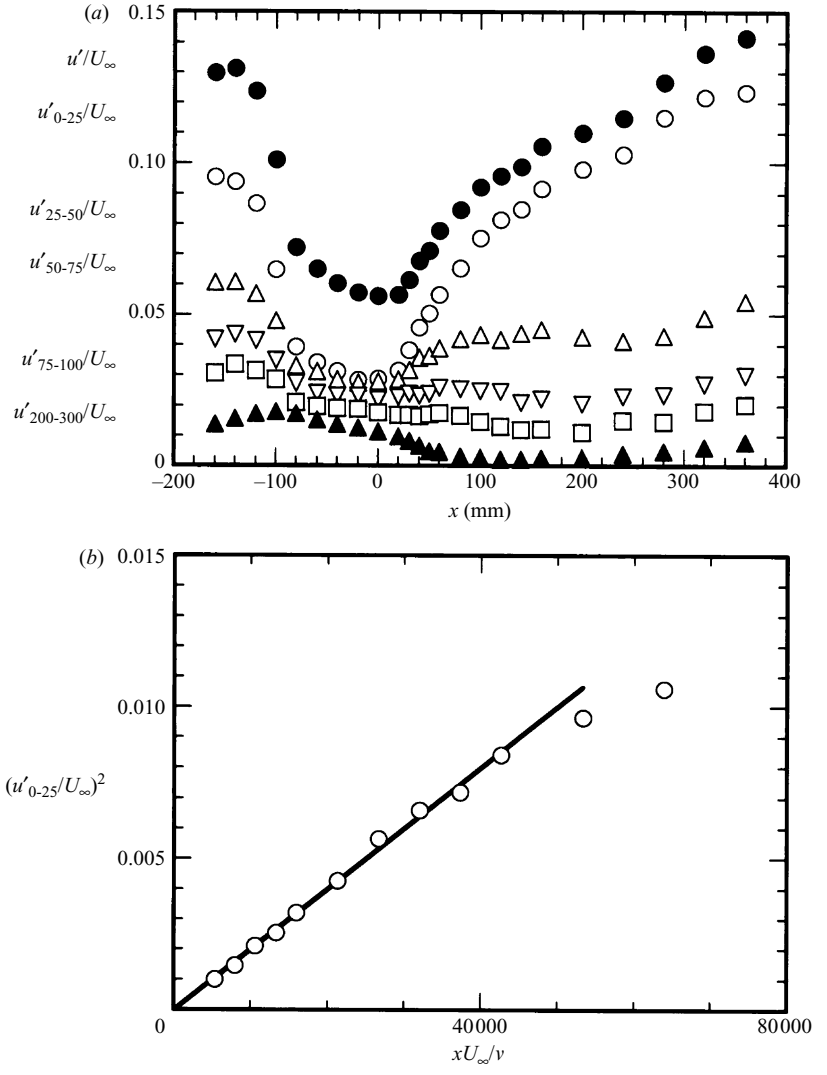

FIGURE 8. Streamwise development of each spectral component at $y = 1$ mm for $V_s/U_\infty = 10\,\%$. (*a*) ●, u'; ○, u'_{0-25}; △, u'_{25-50}; ▽, u'_{50-75}; □, u'_{75-100}; ▲, $u'_{200-300}$. (*b*) u'^2_{0-25} versus xU_∞/ν; solid line, $(u'_{0-25}/U_\infty)^2 = 2 \times 10^{-7}(xU_\infty/\nu)$.

only after the low-frequency component u'_{0-25} exceeds 10 % of U_∞. Thus, the dominant contribution to the total u-fluctuations u' comes from the low-frequency component below 25 Hz growing in the initial stage of the re-transition. By plotting u'^2_{0-25} against xU_∞/ν for $x \leqq 240$ mm, figure 8(*b*) also demonstrates the streamwise growth of the dominant low-frequency component. We see a linear relationship between u'^2_{0-25} and x until u'_{0-25} exceeds 10 % of U_∞. The initial growth is thus not exponential but algebraic, and is expressed as $(u'_{0-25}/U_\infty)^2 = A(xU_\infty/\nu)$ with $A = 2 \times 10^{-7}$. u'_{0-25} (or u') measured at $y = 1$ mm corresponds to the maximum r.m.s. value of its y-distribution at least for $x \leqq 160$ mm ($xU_\infty/\nu \leqq 43000$). The gradient $A(= 2 \times 10^{-7})$ represents a measure of the algebraic growth rate which depends on the initial disturbance energy. The initial energy is given by the suction-surviving vortices in the present experiment

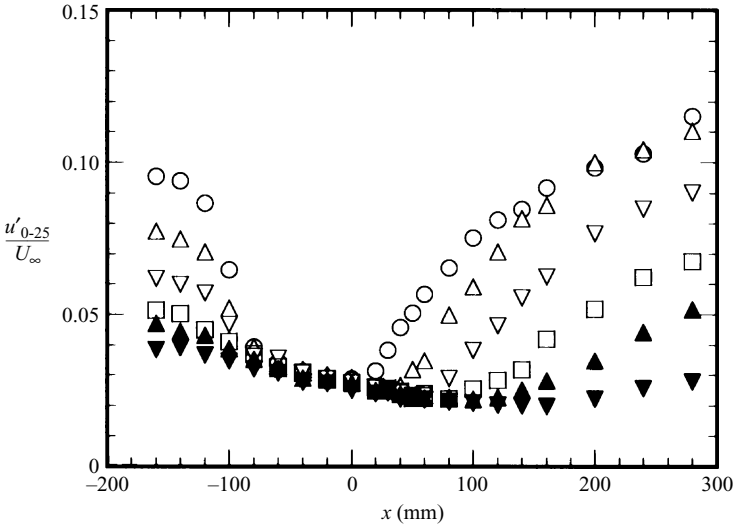

FIGURE 9. Development of u'_{0-25} at various y positions for $V_s/U_\infty = 10\,\%$. ○, $y = 1$ mm; △, $y = 2$ mm; ▽, $y = 3$ mm; □, $y = 4$ mm; ▲, $y = 5$ mm; ▼, $y = 7$ mm.

and by the grid-generated turbulence in Matsubara & Alfredsson (2001). Although we do not obtain data for the initial energy, it may be roughly represented by the value of $(u'_m/U_\infty)^2$ measured at $x = 0$. With this approximation, we find that the growth rate scaled with the initial energy is almost the same as that found by Matsubara & Alfredsson (2001) for the case of grid B (with turbulence level Tu of 1.5 %).

Figure 9 shows the streamwise development of the low-frequency component u'_{0-25} at various y-positions for the case of $V_s/U_\infty = 10\,\%$. Closer to the wall the streamwise growth starts earlier, occurring for $x \geqq 0$ at $y = 1$ mm and for $x \geqq 120$ mm at $y = 6$ mm. These features reflect the lift-up of low-speed fluids, which soon form into streamwise streaks.

4. Generation and growth of near-wall low-speed streaks

We here visualize the near-wall flow immediately upstream, just over and immediately downstream of the suction strip for $V_s/U_\infty = 10\,\%$ in terms of iso-velocity contours of instantaneous streamwise velocity $U + u$ in the (x, z)-plane at $y = 1$ mm, measured by PIV. Figure 10(a) shows the flow field around the leading edge of the suction strip ($-125\,\text{mm} \leqq x \leqq -45\,\text{mm}$), and figure 10($b$) around the trailing edge of the suction strip ($-40\,\text{mm} \leqq x \leqq 40\,\text{mm}$). We can see near-wall low-speed streaks in the turbulent boundary layer approaching the suction strip ($-100\,\text{mm} \leqq x \leqq 0$). When such near-wall streaks enter the suction region, they are sucked out completely, and thus the near-wall flow around the trailing edge of the suction strip becomes laminar without any streaky structure. On the other hand, figures 11(a)–11(d) visualize the near-wall velocity fields downstream of the suction strip for $V_s/U_\infty = 0\,\%$, 5 %, 10 % and 15 %, respectively. All the velocity fields are measured at $y = 1$ mm which corresponds to a height of about 13 wall units ($13\nu/u_\tau$) for the turbulent boundary layer in the absence of suction, and each figure covers the flow field over $x = 20$–100 mm. In the absence of suction, in figure 11(a), we see a zigzag structure of low-speed streaks, typical of the near-wall turbulence. When the boundary-layer suction is applied, streaks disappear completely, as already shown in figure 10.

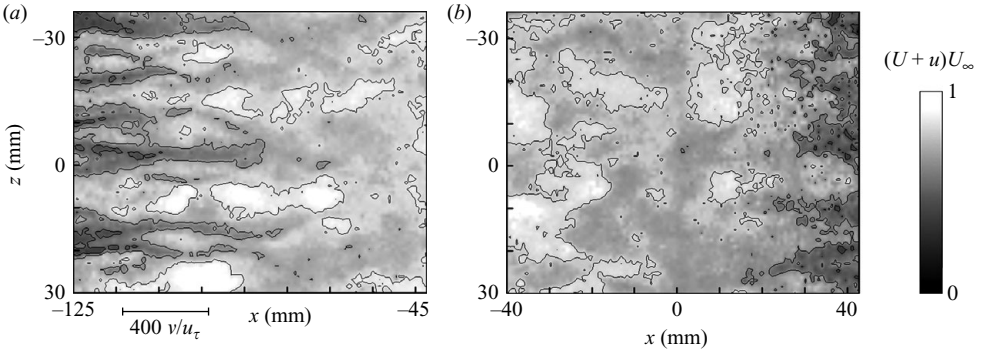

FIGURE 10. Iso-velocity contours of $(U+u)/U_\infty$ at $y=1$ mm for $V_s/U_\infty=10\,\%$. (*a*) Around the leading edge of suction strip; (*b*) around the trailing edge.

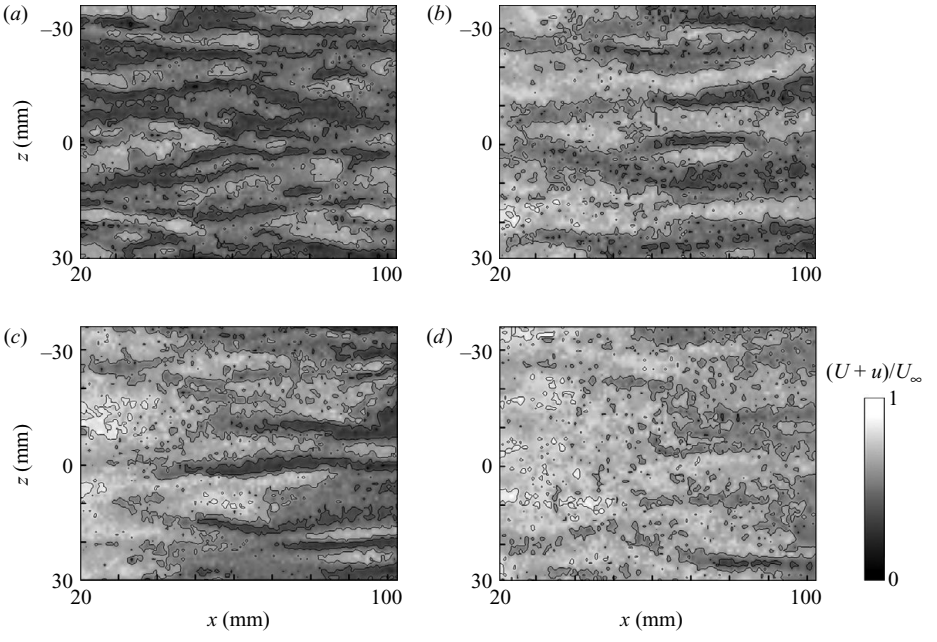

FIGURE 11. Iso-velocity contours of $(U+u)/U_\infty$ at $y=1$ mm. $x=20$–100 mm. (*a*) Without suction; (*b*) $V_s/U_\infty=5\,\%$; (*c*) $V_s/U_\infty=10\,\%$; (*d*) $V_s/U_\infty=15\,\%$.

For the lowest suction rate $V_s/U_\infty=5\,\%$, however, low-speed streaks soon reappear beyond $x=50$ mm as figure 11(*b*) shows. In the other two cases, $V_s/U_\infty=10\,\%$ and 15 %, as shown in figures 11(*c*) and 11(*d*) respectively, their reappearance is delayed further downstream. For $V_s/U_\infty=15\,\%$, we seldom observe distinct low-speed streaks up to $x=100$ mm in figure 11(*d*). Figures 12(*a*) and (*b*), visualizing the near-wall flow beyond $x=100$ mm for $V_s/U_\infty=10\,\%$ and 15 % respectively, show that the newly generated low-speed streaks are very much elongated without any noticeable waviness, though some of the streaks are slightly tilted in the spanwise direction. Their streamwise dimension is more than 80 mm, which corresponds to the low-frequency fluctuations below 25 Hz with the convection velocity of half the free-stream velocity, i.e. $2\,\mathrm{m\,s^{-1}}$. As already shown in figure 8 for $V_s/U_\infty=10\,\%$, the growth of low-frequency fluctuations u'_{0-25} is not exponential but algebraic in the

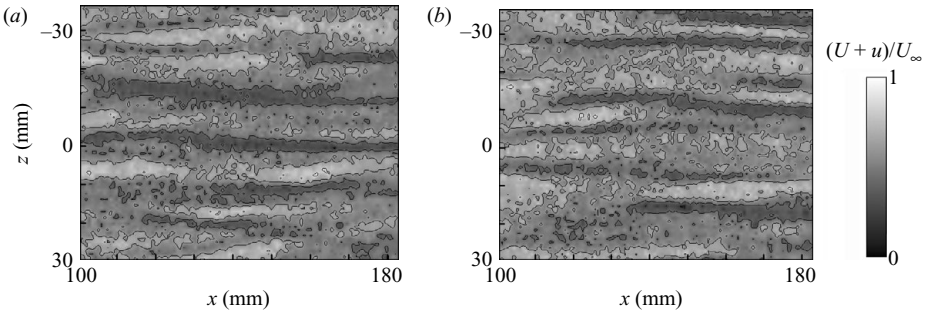

FIGURE 12. Iso-velocity contours of $(U+u)/U_\infty$ at $y=1$ mm, $x=100$–180 mm. (*a*) $V_s/U_\infty=10\,\%$; (*b*) $V_s/U_\infty=15\,\%$.

streamwise direction. The algebraic growth continues until u'_{0-25} exceeds 10 % of U_∞. The low-frequency disturbances (streamwise streaks) attain near-saturation around $x=200$ mm, and immediately behind this location the higher-frequency disturbances start to grow. This suggests that when the low-speed streaks are intensified enough, a secondary instability, known as the streak instability, occurs to lead to sinusoidal oscillations of low-speed streak. For the case of the highest suction rate, $V_s/U_\infty=15\,\%$, figures 11(*d*) and 12(*b*) show that the initial streak growth is so slow that no distinct low-speed streaks appear up to $x=100$ mm, and the re-transition does not occur within the test section up to $x=400$ mm in this case, as already noted in figure 5. Figures 10 and 11 also show that the present suction has no noticeable ill effects such as artificial spanwise variation of near-wall flow. If the present suction were capable of generating spanwise and/or streamwise vortices or any kinds of spatial flow variations, such ill effects would become strong with the suction rate. As a matter of course, by observing the laminar boundary layer (realized without the cylinder trip at $U_\infty=4\,\mathrm{m\,s^{-1}}$) we confirm that no noticeable streaks appear downstream of the suction strip for $V_s/U_\infty=0\,\%$ (without suction), 10 % and 15 %.

No doubt it is the suction-surviving turbulent vortices that generate the low-speed streaks. The maximum r.m.s. value u'_m/U_∞ maintains 6 % at the downstream end of the suction region for $V_s/U_\infty=5\,\%$ and 10 %, being more than 5 % even for $V_s/U_\infty=15\,\%$. Such strong turbulent motions can cause the laminar boundary layer to undergo re-transition through generating low-speed streaks. In a developed turbulent boundary layer, hairpin-like or arch-like vortices are most dominant in the region away from the wall (Robinson 1991; Zhou *et al.* 1999). It is reasonable to infer that when the suction is applied, any vortices otherwise existing in the outer-layer region move towards and close to the wall, and importantly they themselves develop into streamwise vortices through tilting and stretching caused by the intense velocity shear near the wall. So, in order to clarify the process in which turbulent vortices generate the low-speed streaks, we here examine the spanwise velocity component (w) which is closely related to the hairpin and/or streamwise vortices.

Figure 13(*a*) shows the instantaneous w fields near the wall ($y=1$ mm) around the trailing edge of the suction strip (over the region $-40\,\mathrm{mm}\leqq x\leqq 40\,\mathrm{mm}$) for $V_s/U_\infty=10\,\%$, measured simultaneously with the instantaneous streamwise velocity field given in figures 10(*b*). Just over the suction strip, in contrast to the almost complete disappearance of streaky structures in figure 10(*b*), we see many lumps of positive and negative w-fluctuations of more than 10 % of U_∞ in figure 13(*a*). They are not elongated in the streamwise direction and some of them are spot-like. We

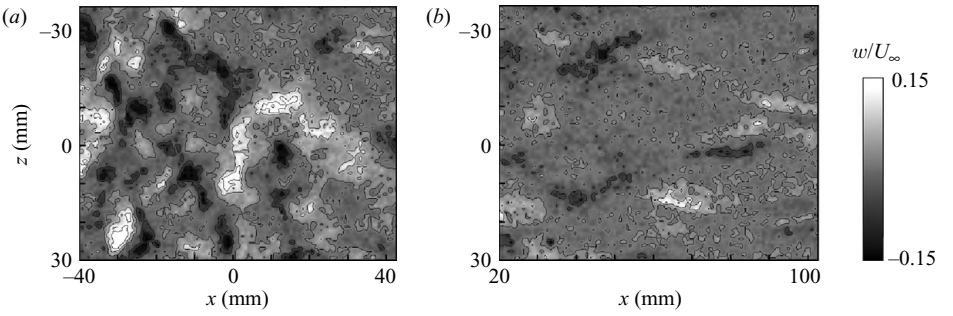

FIGURE 13. Iso-velocity contours of w/U_∞ at $y = 1$ mm for $V_s/U_\infty = 10\,\%$. (*a*) $x = -40$–40 mm; (*b*) $x = 20$–100 mm. These correspond to figures 10(*b*) and 11(*c*).

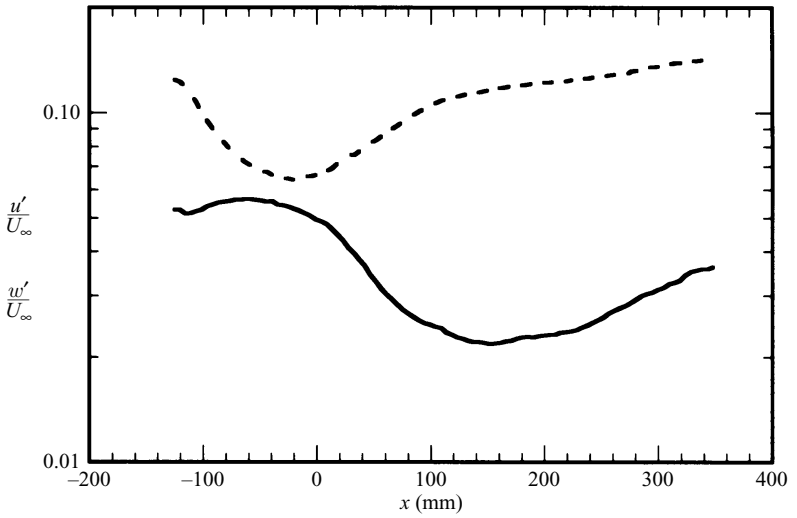

FIGURE 14. Development of u- and w-fluctuations for $V_s/U_\infty = 10\,\%$. The r.m.s. values u' (broken line) and w' (solid line) are obtained from PIV data at $y = 1$ mm.

consider these as features of the turbulent vortices, which existed in the original outer-layer (as hairpin or arch vortices) and now move towards the wall by suction. Figure 13(*b*) shows the instantaneous w fields downstream of the suction, covering the initial growth stage of streamwise streaks around $x = 20$–100 mm. Note that the measurement is made simultaneously with that of the streamwise velocity field given in figure 11(*c*). As the turbulent vortices approach the wall, w-fluctuations soon decay because of viscous effects. Lumps of positive and negative w in figure 13(*b*) become much weaker in intensity than those over the suction strip (figure 13*a*), but are much elongated in the streamwise direction beyond $x = 50$ mm. The elongated lumps of positive and negative w correspond to the streamwise vortices responsible for generating the streamwise streaks shown in figure 11(*c*): see the correspondence between the low-speed streaks and the negative and positive w lumps in figures 11(*c*) and 13(*b*).

Figure 14 shows the streamwise variation of the r.m.s. value w' together with u' obtained from PIV measurements at $y = 1$ mm for $V_s/U_\infty = 10\,\%$. Note that the ordinate is of a logarithmic scale. Over the suction strip, the w' maintains a high intensity, more than 5 % of U_∞, being in sharp contrast to a rapid decrease in

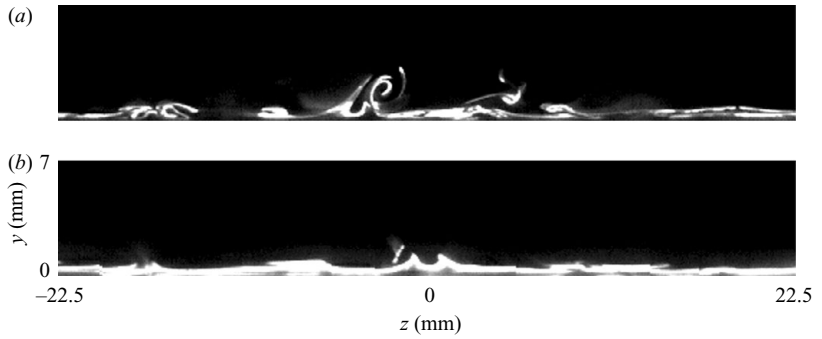

FIGURE 15. Smoke-wire visualization of the near-wall flow for $V_s/U_\infty = 10\,\%$. (*a*) Cross-sectional view at $x = 60\,\text{mm}$; smoke is released from $x = 10\,\text{mm}$. (*b*) Cross-sectional view at $x = 210\,\text{mm}$; smoke is released from $x = 160\,\text{mm}$.

u'. Downstream of the suction, w' decreases rapidly down to about 2.5 % around $x = 150\,\text{mm}$. These features are consistent with the wall suction forcing the turbulent vortices in the original outer layer to move towards the wall. On the other hand, u' increases rapidly, in particular in the region where w' decreases rapidly. This corresponds to the reappearance and growth of streamwise streaks. The low-speed streaks are thus generated by the initially strong but rapidly decaying turbulent vortices. We observe that w' starts to grow beyond $x = 200\,\text{mm}$. This reflects the breakdown of streamwise streaks as we will discuss later.

The streamwise vortices near the wall are more directly visualized by means of a smoke-wire technique. At least qualitatively, smoke visualizations can provide information on a measure of the vortex intensity, namely, the lift-up activity due to the streamwise vortices we are concerned with. For the case of $V_s/U_\infty = 10\,\%$, figure 15(*a*) shows cross-sectional view pictures, where smoke is released from a smoke-wire stretched at $x = 10\,\text{mm}$ and $y = 1\,\text{mm}$, and a laser light sheet (about 1 mm thick) illuminates the cross-section at $x = 60\,\text{mm}$. A strong lift-up of the near-wall smoke is due to streamwise vortices. These primary streamwise vortices decay downstream, as mentioned above. Then the vertical induced velocity is much reduced, and smoke is not strongly concentrated into streak patterns. Indeed, when smoke is released at $x = 160\,\text{mm}$ and $y = 1\,\text{mm}$, the lift-up is weak without accompanying clear roll-up (see figure 15*b*). Such weak streak patterns visualized by smoke are not inconsistent with the behaviour of w' (up to $x = 200\,\text{mm}$) in figure 14.

Next examined is the spanwise spacing of near-wall low-speed streaks in the re-transition region. Figure 16 shows the probability density histograms of the streak spacing λ at $x = 140\,\text{mm}$ for the three cases of $V_s/U_\infty = 5\,\%$, 10 % and 15 % by comparing with that of the fully developed turbulent boundary layer without the suction. Here, the histograms are obtained on the basis of PIV data for the instantaneous velocity field in the (x, z)-plane near the wall and the abscissa is in wall units using the friction velocity u_τ for the developed turbulent flow without suction. The total number of samples N_0 is more than 3000 for each case. Here, we define the low-speed streak as a streaky region where the streamwise velocity is lower than the mean velocity (averaged in the spanwise direction at a fixed y-position). For the case of a fully developed turbulent boundary layer, the probability density of the streak spacing is represented well by a log-normal distribution as reported by several authors (e.g. Smith & Metzler 1983). This is the case for the present turbulent boundary layer

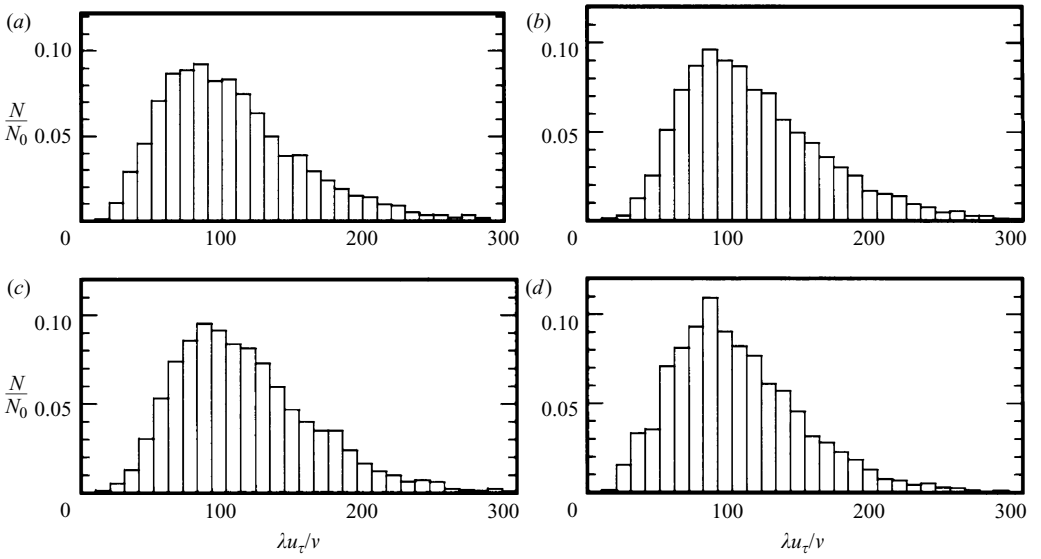

FIGURE 16. Probability density histogram of the streak spacing λ at $x = 140$ mm. (*a*) No suction; (*b*) $V_s/U_\infty = 5\,\%$; (*c*) $V_s/U_\infty = 10\,\%$; (*d*) $V_s/U_\infty = 15\,\%$.

without suction as can be seen from figure 16(*a*), where the spacing is distributed around the most probable value $\lambda_m u_\tau/\nu$ between 80 and 90. The mean value $\bar{\lambda} u_\tau/\nu$ is about 105, which is 20 % larger than the most probable value. The mean value $\bar{\lambda} u_\tau/\nu$ is slightly larger than the well-known value 100. This is reasonable because the measurements are made at $y^+(= yu_\tau/\nu) \approx 13$ ($y = 1$ mm), slightly outsides the viscous sublayer. The spacing of the downstream streaky structure observed is different from the spanwise interval of cylinders (5 mm). If the cylinder trip were serving as anchors for downstream streamwise vortices, it would be impossible for the flow to realize such a histogram scaled with wall units as shown in figure 16(*a*). By checking the spanwise distributions of U near the wall, we confirm that directly cylinder-induced stationary streamwise vortices (if any) have no noticeable effects on the results.

As for the re-transitional boundary layer downstream of the suction, in particular for the cases of $V_s/U_\infty = 5\,\%$ and 10 %, it is remarkable that even at its formation stage (at $x = 140$ mm) the near-wall low-speed streaks exhibit almost the same probability density distribution as that of the developed wall turbulence upstream of the suction. This is consistent with our important observations, first that the low-speed streaks are excited by near-wall streamwise vortices evolving from the suction-surviving turbulent vortices, which have the same spatial scale as the developed wall turbulence, and secondly that the near-wall shear in the re-transitional flow is almost the same as that of the developed wall turbulence, as we see from figures 3(*b*), 3(*c*) and 3(*d*) for $x = 50$ mm, 150 mm and 250 mm, respectively. These observations suggest that at the initial stage of re-transition, the streamwise vortices govern the near-wall momentum transfer and cooperate with the viscous stress to determine the near-wall shear, which in turn governs the scales of streamwise vortices and low-speed streaks.

Figure 17 plots the mean velocity profile for the higher suction rate $V_s/U_\infty = 15\,\%$ and the Blasius profile in such a way that the near-wall shears coincide with each other. The Blasius profile represents the present data well. The displacement thickness of the laminar layer δ^* is 1.6 mm at $x = 150$ mm. The most-probable value of λ_m (about 6 mm) is thus about four times the displacement thickness. In this respect, we refer

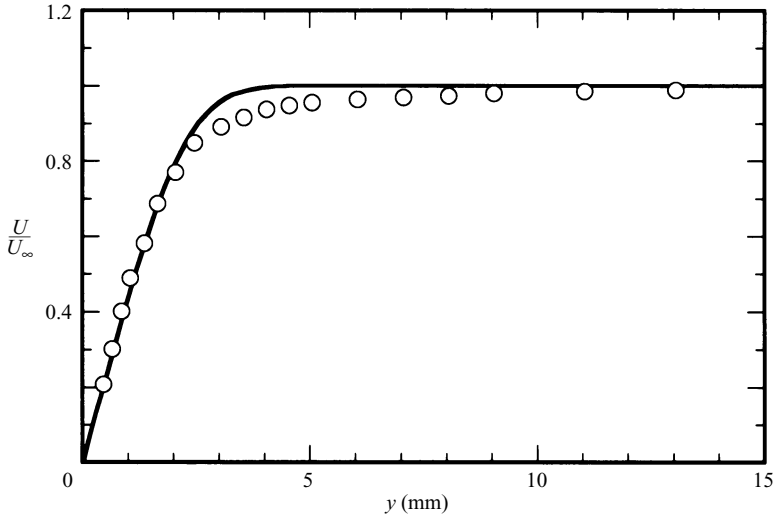

FIGURE 17. Comparison of mean velocity distribution at $x = 150$ mm for $V_s/U_\infty = 15\,\%$ (○) with Blasius flow profile (solid curve).

to the optimal disturbance theory cited earlier (Andersson *et al.* 1999; Luchini 2000). The theory predicts that the optimal perturbation excites such streamwise streaks as characterized by a lateral spacing of about eight times the displacement thickness. In the present experiment, the streaks are excited by the suction-surviving strong vortices and the probability density of the spanwise spacing is found to be distributed around half of the value predicted by the linear optimal disturbance theory. From figure 16(*d*), we see that the probability density N/N_0 is less than 0.01 for the theoretical optimum spacing (corresponding to 200 in wall units), while it is about 0.1 around the most probable spacing near 100 in wall units. In the subcritical boundary-layer transition caused by high-intensity hairpin eddies (Asai & Nishioka 1995), the spanwise spacing was found to be about four times the displacement thickness, the same as in the present experiment. Matsubara & Alfredsson (2001) also observed almost the same discrepancy between their experiments and the theory.

5. Breakdown of near-wall low-speed streaks

We describe the breakdown of low-speed streaks in this section. Low-frequency u-fluctuations undergo the algebraic growth, and high-frequency disturbances start to grow when the low-frequency components exceed about 10 % of U_∞ in r.m.s. value (see figure 8). Correspondingly, as shown in figure 14, w-fluctuations are beginning to grow. These suggest that the streak instability has set in at this stage. The streak instability is excited by random disturbances and leads to the streak breakdown.

We first visualize the flow field beyond $x = 250$ mm by means of PIV and smoke wire. Smoke-wire visualizations emphasize the occurrence of spanwise oscillations of streaks, namely the streak breakdown. We want to see whether such breakdown is governed by the streak instability or not. Figures 18(*a*) and 18(*b*), respectively, show the instantaneous streamwise and spanwise velocity contours near the wall, which are simultaneously measured at $y = 1$ mm by PIV. By conducting a double Fourier analysis of the instantaneous w field measured by PIV, we cut off the contributions

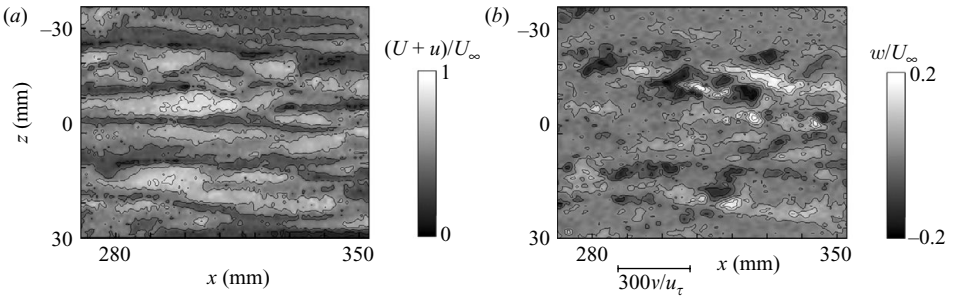

FIGURE 18. Iso-velocity contours of the streamwise and spanwise velocities simultaneously measured by PIV at $y = 1$ mm over $x = 265$–350 mm for $V_s/U_\infty = 10\,\%$. (a) Streamwise velocity ($U + u$); (b) spanwise velocity (w).

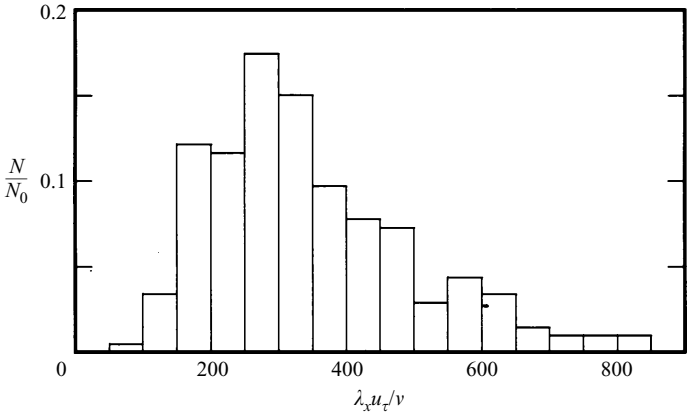

FIGURE 19. Probability density histogram of the streamwise wavelength λ_x of the secondary streak instability for $V_s/U_\infty = 10\,\%$.

of small-scale fluctuations which are shorter than 7 mm (about 93 in wall units) in streamwise wavelength. This is because we have to visualize the spanwise velocity fluctuations (w) that are associated with the coherent streamwise vortices. Figure 18(a) shows clear patterns of sinusoidal oscillations in some of low-speed streaks (around $z = -12$ mm and -20 mm). In figure 18(b), positive and negative w-velocity lumps are alternatively aligned along the wavy low-speed streaks. These indicate the occurrence of the same sinuous instability as we observed under well-controlled disturbance conditions (see Asai *et al.* 2002). The wavelength, defined as the distance between neighbouring positive (or negative) lumps, is found to be about 23 mm in this case, which is equal to about 300 ν/u_τ where the value of the fully developed turbulent flow is used for the friction velocity u_τ. In the present experiment, many PIV pictures (more than 200 out of the total 500 pictures) show clear patterns of the sinuous instability so that we can obtain the histogram for the streamwise wavelength non-dimensionalized with ν/u_τ. The result is shown in figure 19. The most probable value is around 300 in wall units, which corresponds to the most amplified disturbance calculated from the liner stability by Schoppa & Hussain (2002) on the basis of the streak flow deduced from DNS data for wall turbulence.

The streak instability is of a convective nature (Brandt *et al.* 2003). It is excited by suction-surviving turbulent fluctuations in the present case. The streak instability and its subsequent breakdown occur at random in space and time in spite of the spanwise arrangement of streaks being almost periodic. The wavetrain that the streak instability develops is rather short, with no more than two waves for the most cases. According to experimental observations by Lundell (2004), such localized disturbances do not undergo exponential growth, unlike long wavetrains and the growth rate is considerably reduced on decreasing the number of waves to below two. In the present experiment, the spatial amplification rate of w' is estimated from figure 14 for a streamwise distance of 1000 in wall units, namely for $x = 240$–320 mm. The amplification rate (i.e., the ratio of amplitude at $x = 320$ mm to that at $x = 240$ mm) is about 1.4, being really small, which is probably due to the effect of short wave packet.

The local streak instability is further examined by means of smoke-wire visualization for the case of $V_s/U_\infty = 10\,\%$. By focusing on the behaviour of low-speed streaks, we attempt to capture a sequence of events characterizing the sinuous streak instability and an example of such results is shown in figure 20. Smoke is released from a smoke wire stretched at $(x,\ y) = (250\,\text{mm},\ 1\,\text{mm})$, and the top-view pictures are taken by using a digital high-speed video camera. The time interval between two consecutive pictures is 2.5 ms. Streaks of concentrated smoke represent the low-speed streak. We see that some of them undergo sinuous spanwise motions. These sinuous motions are amplified as convecting downstream, indicating the convective nature of the streak instability. In these pictures, the streamwise wavelength of the streak instability is also found to be three times the mean streak spacing, i.e. about $300\nu/u_\tau$. The wavy pattern is travelling at a speed of half the free-stream velocity U_∞. Figure 21 shows a time sequence of the cross-sectional view pictures at the breakdown stage for $V_s/U_\infty = 10\,\%$. Smoke is released at $x = 250$ mm and a laser light sheet (about 1 mm thick) illuminates a cross-section at $x = 300$ mm. The time interval between two consecutive pictures is 1 ms. It is demonstrated that the whole smoke-visualized flow is dominated by energetic mushroom-like structures and their induced fields that are violently oscillating in the spanwise direction. The time period of the lateral oscillation is about 10 ms or about 30 in wall units, which corresponds to the sinuous instability shown in figure 20. With these results, we may say that the sign-alternating w-velocity patterns along the wavy streamwise streaks (for $z = -12$ mm to -20 mm) in figure 18(*b*) are the evidence for the quasi-streamwise vortices such as illustrated in figure 22 that are generated by the streak instability and its nonlinear development. As we see below, the log-law profile appears in the mean velocity distribution as the near-wall activities shown in figures 20 to 22 are intensified. These features are almost the same as those of the streak breakdown observed in our previous experiments of the streak instability (Asai *et al.* 2002). It is also remarkable that the quasi-streamwise vortices generated by the streak instability in the present experiment are indistinguishable from the dominant near-wall vortices emphasized by Schoppa & Hussain (1997) and Jiménez & Pinelli (1999) as the key structure governing the self-sustaining mechanism of wall turbulence.

Finally, we describe the mean velocity field. Figure 23 plots the mean velocity distributions $U(y)$ at four stations, $x = 20$ mm, 150 mm, 250 mm and 350 mm for $V_s/U_\infty = 5\,\%$. The log-law distribution is included for comparison. At $x = 20$ mm and 150 mm, the velocity distributions exhibit a quasi-laminar profile near the wall, while the outer region still keeps the characteristics of turbulent boundary layer even after the suction. At $x = 250$ mm, despite the streak instability already beginning with increasing wall bursts there, the mean velocity is still far from the log-law distribution.

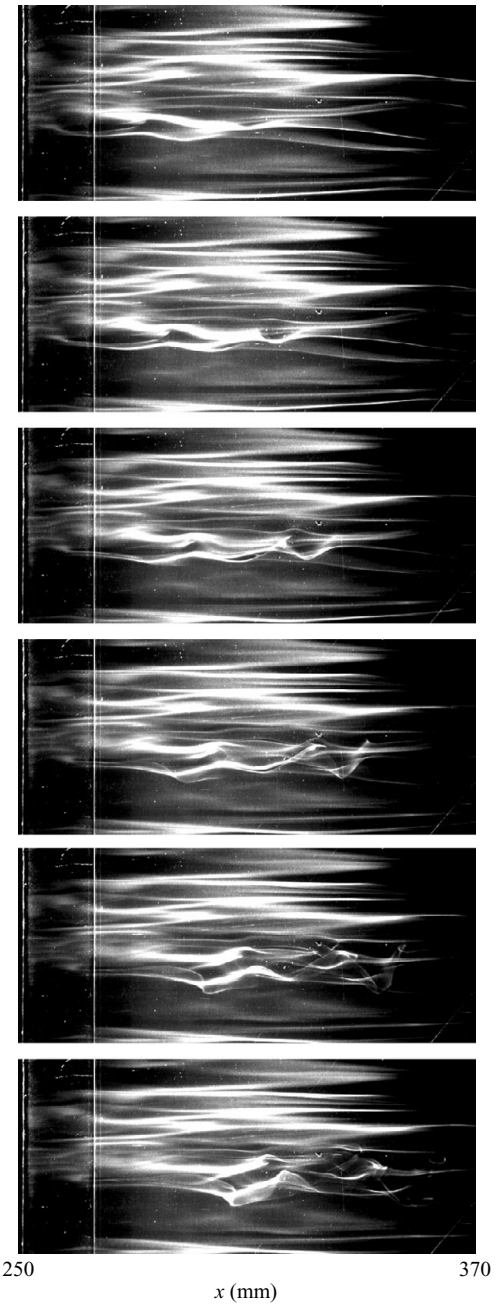

FIGURE 20. Smoke-wire visualization of the near-wall flow for $V_s/U_\infty = 10\,\%$. Smoke is released from $(x,\ y) = (250\,\text{mm},\ 1\,\text{mm})$. Time increases from top to bottom, the interval between two consecutive pictures being 2.5 ms.

It is beyond $x = 350\,\text{mm}$, where the streak breakdown has further proceeded, that the log-law region appears in the velocity distribution. The tendency of the mean velocity towards the turbulent profile is similar to the result reported by Antonia & Zhu (1995). The present study shows that the instability and breakdown of near-wall

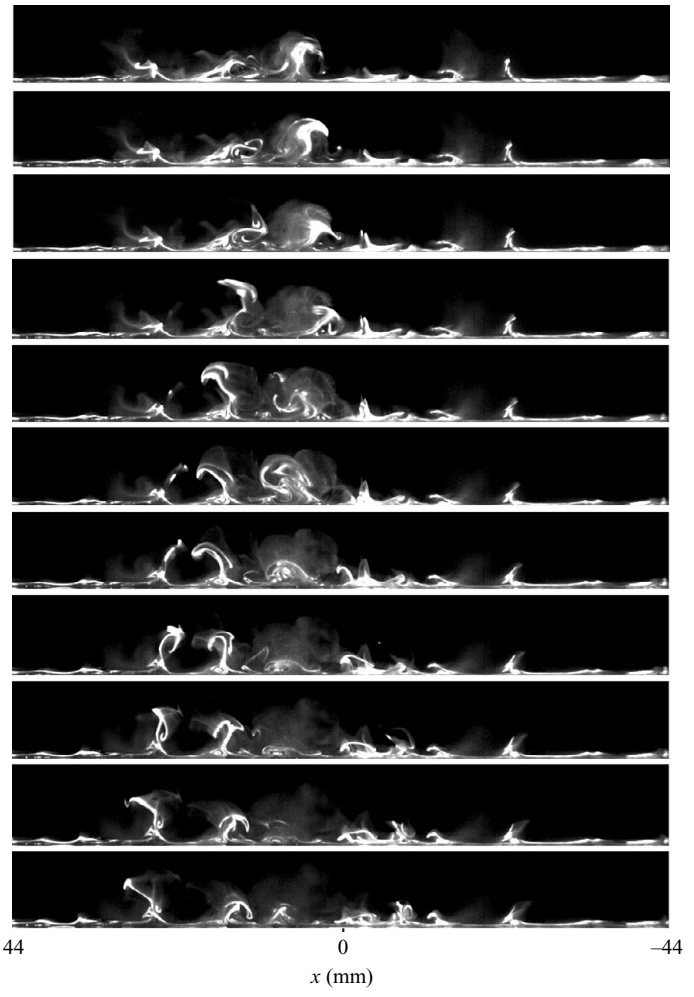

FIGURE 21. Smoke-wire visualization of the near-wall flow for $V_s/U_\infty = 10\,\%$. Cross-sectional view at $x = 300\,\text{mm}$. Smoke is released from $x = 250\,\text{mm}$. Time increases from top to bottom, the interval between two consecutive pictures being 1 ms.

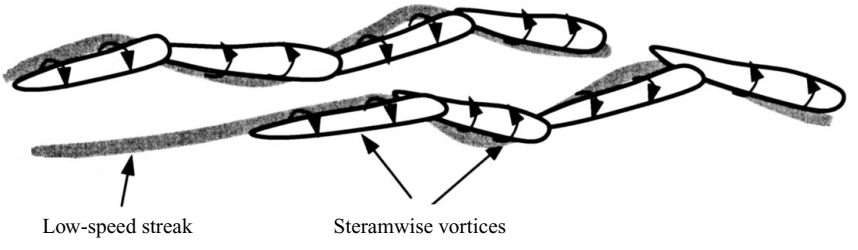

FIGURE 22. Schematic of the instability and breakdown of low-speed streaks observed for $x = 280\,\text{mm}$ to 330 mm and $z = -12\,\text{mm}$ to $-20\,\text{mm}$ in figure 18.

low-speed streaks almost directly give rise to the wall-turbulence mechanism responsible for the appearance of the log-law profile. Transition experiments by Nishioka *et al.* (1981) and Nishioka & Asai (1984) show that the near-wall streak and wall-burst activities lead to the appearance of the log-law profile.

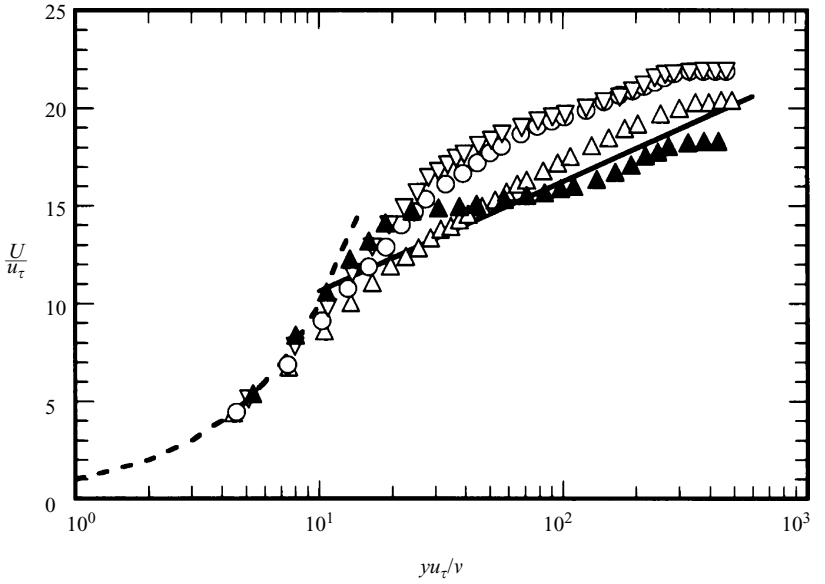

FIGURE 23. Mean velocity distributions at $x = 20$ mm (▲), 150 mm (▽), 250 mm (○) and 350 mm (△) for $V_s/U_\infty = 5\,\%$. Solid line, $U/u_\tau = 5.62\ln(yu_\tau/\nu) + 5.0$; broken line, $U/u_\tau = yu_\tau/\nu$.

6. Concluding remarks

In the present experimental study, two-dimensional local wall suction is applied to a fully developed turbulent boundary layer such that near-wall turbulence structures are completely sucked out, but most of the turbulent vortices in the original outer layer can survive the suction and cause the resulting laminar flow to undergo re-transition. This has enabled us to examine two important stages of the wall-turbulence generation, that is, the formation of low-speed streaks caused by the suction-surviving turbulent vortices and the subsequent breakdown of streaks. A sequence of events observed in the re-transition is summarized in figure 24.

Near-wall low-speed streaks in the oncoming turbulent boundary layer disappear immediately downstream of the suction strip. When the suction rate is not large, however, turbulent vortices in the core of the oncoming turbulent boundary layer can survive the suction. In terms of u'/U_∞ and w'/U_∞, the intensity of the suction-surviving turbulent vortices is, respectively, about 6 % and 5 % at the downstream end of the suction strip. Such still active turbulent vortices (originally being in the outer layer) penetrate deep into the near-wall region and the near-wall intense velocity shear forces them to evolve into streamwise vortices, which then cause low-speed streaks. The low-speed streaks thus generated are much elongated and their spanwise arrangement is rather regular in spite of them being excited by random turbulent vortices. The growth of low-speed streaks manifests itself as the growth of low-frequency velocity fluctuations near the wall. The hot-wire measurements indicate that low-frequency velocity fluctuations once suppressed by the suction soon start to grow algebraically downstream of the suction strip. It is emphasized that while generating low-speed streaks, the streamwise vortices themselves keep decaying downstream. These features in the development of low-speed streaks are not inconsistent with the concept of the regeneration cycle of wall turbulence (Jiménez & Pinelli 1999).

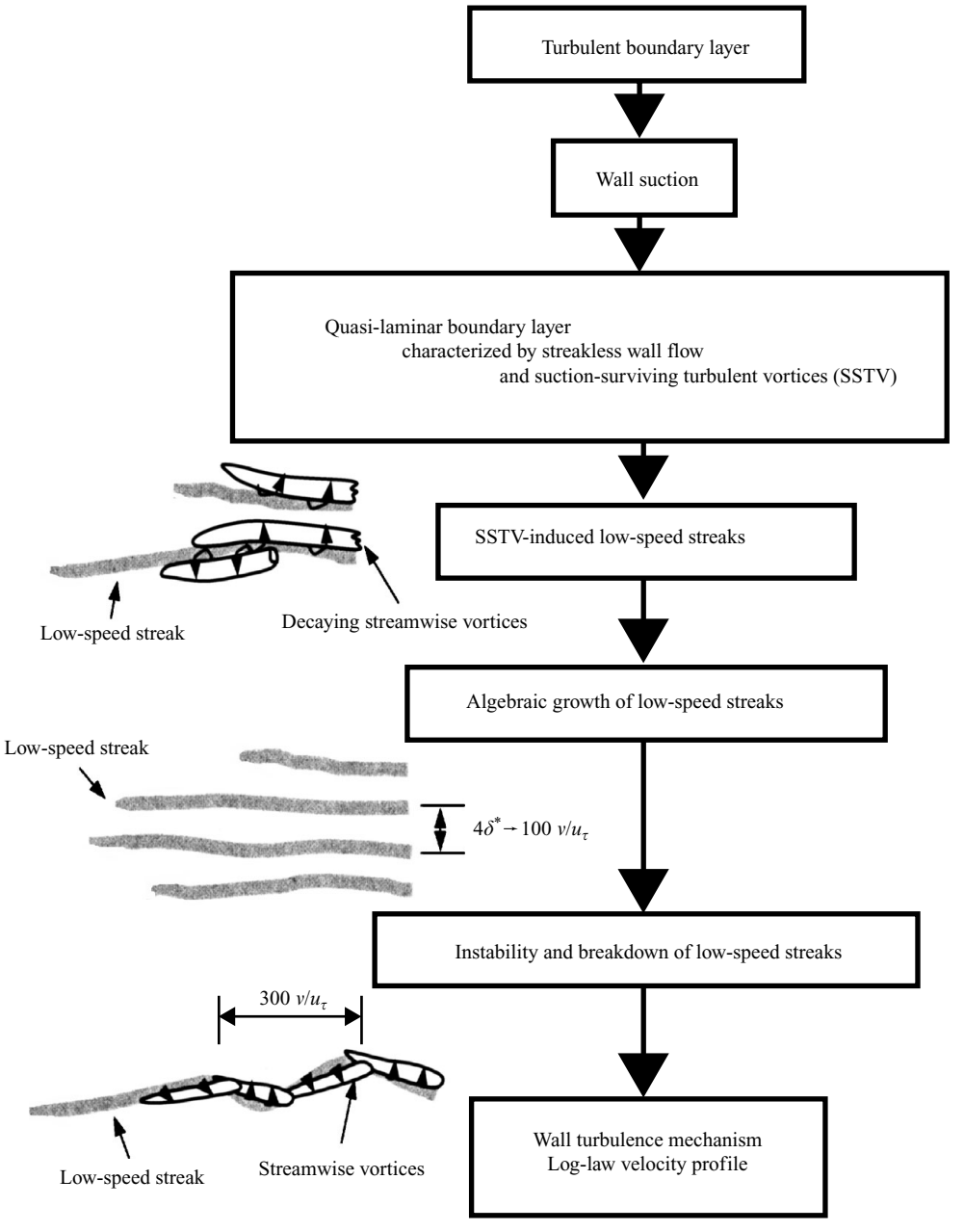

FIGURE 24. A sequence of events giving rise to wall turbulence in the present re-transition.

The optimal transient growth theory predicts for the Blasius boundary layer that the optimal streaks have a spamwise spacing of about eight times the displacement thickness. This is in sharp contrast to our observations where the mean spacing is about four times the displacement thickness, being of the order of the boundary-layer thickness. At the lowest critical Reynolds number for the subcritical transition in plane channel flow, the streak spacing is found to be almost twice the channel

half-depth, corresponding to the boundary-layer thickness, as shown by Nishioka & Asai (1985). As already noted, Asai & Nishioka (1995) observed the spacing to be four times the displacement thickness for the case of subcritical transition in Blasius flow. In Blasius flow, the spanwise vorticity is distributed mainly within a wall layer of twice the displacement thickness. In the present experiment, figures 3(*b*) and 3(*c*) indicate that the wall layer of high shear has almost the same thickness for the four cases independently of the suction rate, including the case without suction. Correspondingly, as shown in figure 16, the probability density histogram of the streak spacing is almost the same for the four cases independently of the suction rate. These results strongly suggest that the streak spacing is about twice the thickness of the wall shear layer, whether the flow state is laminar or turbulent. In turbulent boundary layers, the streamwise vortices govern the near-wall momentum transfer and cooperate with the viscous stress to determine the wall shear layer, which in turn governs the scales of streamwise vortices and low-speed streaks. In this case, the thickness of the wall layer is 50, and the streak spacing is 100 in wall units. It is further noted that for the case of the cited channel flow subcritical transition, the channel half-depth is about 50 in wall units at the lowest critical Reynolds number (see Nishioka & Asai 1985).

The breakdown of low-speed streaks is mainly caused by the streak instability in the present disturbance environment where the turbulent intensity triggering the instability is of the order of 2.5 % in terms of w'/U_∞, that is half the value in the developed wall turbulence. The breakdown occurs unless the momentum thickness Reynolds number is reduced by suction below a critical value. Our flow visualization indicates that the sinuous streak instability mode develops into a train of streamwise vortices with sign-alternating vorticity, as already demonstrated in many papers since Jeong *et al.* (1997). The streak instability starts to occur when the low-speed streaks are intensified such that the r.m.s. value of the associated low-frequency u-fluctuations increases beyond 10 % of U_∞. By observing the y-extent of the low-frequency fluctuations in figure 9, we estimate the height of the low-speed streak to be about half the streak spacing at the onset of the streak instability. It should be stressed that the geometry of the low-speed streaks developing in the re-transition process is similar to that observed in the wall turbulence. The streamwise wavelength of the subsequent streak instability, around 300 in wall units, is close to the prediction from the linear stability analysis by Schoppa & Hussain (2002) for the typical streaks in the wall turbulence. However, the instability event occurs locally in space (both in the streamwise and spanwise directions) and time, and the wavetrain is short, with fewer than two waves, suggesting that the instability leading to the streak breakdown should be analysed for highly-localized wave packets under turbulent fluctuations.

On increasing the suction rate, the growth of low-speed streaks in the re-transition region is made less intense and the eventual breakdown is delayed further downstream because the thinning of the near-wall shear layer (or decrease in the momentum thickness Reynolds number R_θ) stabilizes the near-wall flow. For instance, in the case of $V_s/U_\infty = 15\,\%$, R_θ decreases to below 200. Under such conditions, although the surviving turbulent vortices can still generate near-wall low-speed streaks, the resulting low-speed streaks are only elongated and decaying downstream without being intensified up to the stage of the streak instability. Thus, it may be emphasized that the generation (or regeneration) process of the near-wall low-speed streaks, particularly the transient growth of streaks is highly viscosity-conditioned at low Reynolds numbers close to the minimum transition Reynolds number (of wall-bounded shear flows), $R_\theta = 100$–150.

This work was in part supported by the Grant-in-Aid for Scientific Research (no. 10650897) from Japan Society for the Promotion of Science, the Grant-in-Aid for Scientific Research on Priority Area (no. 12125203) from the Ministry of Education, Culture, Sports, Science and Technology of Japan.

REFERENCES

Andersson, P., Berggren, M. & Henningson, D. S. 1999 Optimal disturbances and bypass transition in boundary layers. *Phys. Fluids* **11**, 134–150.

Andersson, P., Brandt, L., Bottaro, A. & Henningson, D. S. 2001 On the breakdown of boundary layer streaks. *J. Fluid Mech.* **428**, 29–60.

Antonia, R. A. & Zhu, Y. 1995 Effect of concentrated wall suction on a turbulent boundary layer. *Phys. Fluids* **7**, 2465–2474.

Asai, M. & Nishioka, M. 1995 Boundary layer transition triggered by hairpin eddies at subcritical Reynolds numbers. *J. Fluid Mech.* **297**, 101–123.

Asai, M. & Nishioka, M. 1997 Development of wall turbulence structure in transitional flows. In *Theoretical and Applied Mechanics 1996* (ed. R. Tatsumi, T. Kambe & E. Watanabe), pp. 121–138. Elsevier.

Asai, M., Minagawa, M. & Nishioka, M. 2000 Instability and breakdown of the three-dimensional high-shear layer associated with a near-wall low-speed streak. In *Laminar–Turbulent Transition* (ed. H. S. Fasel & W. S. Saric), pp. 269–274. Springer.

Asai, M., Minagawa, M. & Nishioka, M. 2002 The instability and breakdown of the near-wall low-speed streak. *J. Fluid Mech.* **455**, 289–314.

Brandt, L. 2007 Numerical studies of the instability and breakdown of a boundary-layer low-speed streak. *Euro. J. Mech.* B/*Fluids* **26**, 64–82.

Brandt, L. & Henningson, D. S. 2002 Transition of streamwise streaks in zero-pressure-gradient boundary layers. *J. Fluid Mech.* **472**, 239–261.

Brandt, L., Cossu, C., Chomaz, J. M., Huerre, P. & Henningson, D. S. 2003 On the convectively unstable nature of optimal streaks in boundary layers. *J. Fluid Mech.* **485**, 221–242.

Elofsson, P. A., Kawakami, M. & Alfredsson, P. H. 1999 Experiments on the stability of streamwise streaks in plane Poiseuille flow. *Phys. Fluids* **11**, 915–930.

Fransson, J. H. M., Brandt, L., Taramelli, A. & Cossu, C. 2004 Experimental and theoretical investigation of the nonmodal growth of steady streaks in a flat plate boundary layer. *Phys. Fluids* **16**, 3627–3637.

Hamilton, J. M., Kim, J. & Waleffe, F. 1995 Regeneration mechanisms of near-wall turbulence structures. *J. Fluid Mech.* **287**, 317–348.

Hultgren, L. S. & Gustavsson, L. H. 1981 Algebraic growth of disturbances in a laminar boundary layer. *Phys. Fluids* **24**, 1000–1004.

Itano, T. & Toh, S. 2001 The dynamics of bursting process in wall turbulence. *J. Phys. Soc. Japan* **70**, 703–716.

Jeong, J. & Hussain, F. 1995 On the identification of a vortex. *J. Fluid Mech.* **285**, 69–94.

Jeong, J., Hussain, F., Schoppa, W. & Kim, J. 1997 Coherent structures near the wall in a turbulent channel flow. *J. Fluid Mech.* **332**, 185–214.

Jiménez, J. & Moin, P. 1991 The minimal flow unit in near-wall turbulence. *J. Fluid Mech.* **225**, 213–240.

Jiménez, J. & Pinelli, A. 1999 The autonomous cycle of near-wall turbulence. *J. Fluid Mech.* **389**, 335–359.

Kawahara, G. & Kida, S. 2001 Periodic motion embedded in plane Couette turbulence: regeneration cycle and burst. *J. Fluid Mech.* **449**, 291–300.

Konishi, Y. & Asai, M. 2004 Experimental investigation of the instability of spanwise-periodic low-speed streaks. *Fluid Dyn. Res.* **34**, 299–315.

Landahl, M. T. 1980 A note on an algebraic instability of inviscid parallel shear flows. *J. Fluid Mech.* **98**, 243–251.

Luchini, P. 2000 Reynolds-number-independent instability of the boundary layer over a flat surface: optimal perturbations. *J. Fluid Mech.* **404**, 289–309.

Lundell, F. 2004 Streak oscillations of finite length: disturbance evolution and growth. *Phys. Fluids* **16**, 3227–3230.

Matsubara, M. & Alfredsson, P. H. 2001 Disturbance growth in boundary layers subjected to free stream turbulence. *J. Fluid Mech.* **430**, 149–168.

Narasimha, R. & Sreenivasan, K. R. 1973 Relaminarization in highly accelerated/turbulent boundary layers. *J. Fluid Mech.* **61**, 417–447.

Nishioka, M. & Asai, M. 1984 Evolution of Tollmien–Schlichting waves into wall turbulence. In *Turbulence and Chaotic Phenomena in Fluids* (ed. T. Tatsumi), pp. 87–92. North-Holland.

Nishioka, M. & Asai, M. 1985 Some observations of the subcritical transition in plane Poiseuille flow. *J. Fluid Mech.* **150**, 441–450.

Nishioka, M., Asai, M. & Iida, S. 1981 Wall phenomena in the final stage of transition to turbulence. In *Transition and Turbulence* (ed. R. E. Meyer), pp. 113–126. Springer.

Reddy, S. C., Schmid, P. J., Baggett, J. S. & Henningson, D. S. 1998 On the stability of streamwise streaks and transition thresholds in plane channel flows. *J. Fluid Mech.* **365**, 269–303.

Robinson, S. K. 1991 Coherent motions in the turbulent boundary layer. *Annu. Rev. Fluid Mech.* **23**, 601–639.

Schoppa, W. & Hussain, F. 1997 Genesis and dynamics of coherent structures in near-wall turbulence: a new look. In *Self-Sustaining Mechanisms of Wall Turbulence* (ed. R. L. Panton), chap. 16, pp. 385–422. Computational Mechanics.

Schoppa, W. & Hussain, F. 2002 Coherent structure generation in near-wall turbulence. *J. Fluid Mech.* **453**, 57–108.

Smith, C. R. & Metzler, S. P. 1983 The characteristics of low-speed streaks in the near-wall region of a turbulent boundary layer. *J. Fluid Mech.* **129**, 27–54.

Tumin, A. & Reshotko, E. 2001 Spatial theory of optimal disturbances in boundary layers. *Phys. Fluids* **13**, 2097–2104.

White, E. B. 2002 Transient growth of stationary disturbances in a flat plate boundary layer. *Phys. Fluids* **14**, 4429–4439.

Zhou, J., Adrian, R. J., Balachandar, S. & Kendall, T. M. 1999 Mechanisms for generating coherent packets of hairpin vortices in channel flow. *J. Fluid Mech.* **387**, 353–396.